Am J Cancer Res 2022;12(6):2558-2575
www.ajcr.us /ISSN:2156-6976/ajcr0141670

Original Article

TDO2 and tryptophan metabolites promote kynurenine/AhR signals to facilitate glioma progression and immunosuppression

Chuanhong Zhong[1,2], Lilei Peng[1,2], Bei Tao[3], Senlin Yin[4], Liang Lyu[4], Hao Ding[5], Xiaobo Yang[1,2], Tangming Peng[1,2], Haiping He[1,2], Peizhi Zhou[4]

[1]Department of Neurosurgery, The Affiliated Hospital of Southwest Medical University, Luzhou 646000, Sichuan, China; [2]Sichuan Clinic Research Center for Neurosurgery, Luzhou, China; [3]Department of Rheumatism, Affiliated Hospital of Southwest Medical University, Luzhou, Sichuan, China; [4]Department of Neurosurgery, West China Hospital of Sichuan University, Chengdu, Sichuan, China; [5]Neurosurgery Department of The Fourth People's Hospital of Zigong, Zigong, Sichuan, China

Received January 10, 2022; Accepted April 23, 2022; Epub June 15, 2022; Published June 30, 2022

Abstract: Tumor cells exhibit enhanced uptake and processing of nutrients to fulfill the demands of rapid growth of tumor tissues. Tryptophan metabolizing dioxygenases are frequently up-regulated in several tumor types, which has been recognized as a crucial determinant in accelerated tumor progression. In our study, we explored the specific role of tryptophan 2,3-dioxygenase 2 (TDO2) in glioma progression. Analysis of mRNA profiles in 325 glioma patients based on the rich set of CCGA database was performed, which revealed that high TDO2 expression was tightly correlated with poor prognosis in glioma patients. TDO2 increased intracellular levels of tryptophan metabolism in the kynurenine (Kyn) pathway *in vitro* and *in vivo*, resulting in sustained glioma cell proliferation. Mechanistically, overexpression of TDO2 promoted the secretion of Kyn, which in turn stimulated the activation of the aryl hydrocarbon receptor (AhR)/AKT signaling pathway, resulting in heightened proliferative properties and tumorigenic potential in glioma cells. Meanwhile, Kyn produced by tumor cells further suppressed the proliferation of functional T cells, thereby resulting in immunosuppression and enhanced tumor growth in glioma. Our study showed that TDO2-induced increase in tryptophan metabolite Kyn played a pivotal role in glioma development via the AhR/AKT pro-survival signals and immunosuppressive effects, suggesting that the use of TDO2 inhibitors in combination with chemotherapy may be a novel strategy to effectively and synergistically eliminate glioma cells.

Keywords: Tryptophan metabolism, TDO2, kynurenine, AhR, glioma

Introduction

Glioma is one of the most common brain-associated malignant brain tumors, with over 150,000 new diagnoses each year [1-3]. Despite advances in surgical procedures and adjuvant chemotherapy, the prognosis of patients with glioma remains extremely poor due to high incidences of recurrence and sustained tumor growth [4-7]. Moreover, the underlying mechanism of tumor progression in glioma is also poorly understood [8-10]. Herein, there is an imperative demand to develop effective therapeutic strategies targeting and eliminating the neoplastic burden of gliomas.

Metabolic reprogramming is a hallmark of cancer and recognized as a crucial determinant in cancer cell proliferation and tumor progression [11-14]. Alterations in metabolism were found in several cancer cell types, and metabolic coupling between stromal and tumor cells plays crucial roles in cancer development [15-17]. Increasing evidence suggests correlation of tryptophan catabolism with advanced disease stages in cancer patients [18, 19]. The tryptophan metabolites Kyn, including 3-hydroxykynurenine, L-kynurenine, 3-hydroxyanthranilic acid, and quinolinic acid, is known as a crucial participant in inhibiting anticancer immune responses by suppressing the proliferation of functional T cells [20]. The intracellular tryptophan indoleamine-2,3-dioxygenase (IDO) and TDO play central roles in tryptophan metabolism and Kyn production. IDO/TDO activity could be estimated by the Kyn to tryptophan (Kyn/

Trp) ratio [21, 22]. High Kyn/Trp ratio and IDO expression are frequently associated with elevated tumor progression and poor prognosis in cancer patients [19, 23, 24]. The expression of IDO is also thought to be correlated with the regulatory Treg activation in tumor tissues [23, 24]. However, few studies have explored the role of TDO/IDO in glioma. The underlying mechanism of tumor progression induced by TDO-associated tryptophan metabolism remains controversial.

In recent years, AhR has been characterized as a regulator of toxicity and carcinogenic response to environmental cues, including TCDD and aromatic hydrocarbons [25-27]. Compelling studies suggested that AhR participated in important pathological activities, including cell proliferation, cell migration, and tumorigenesis [25-27]. More importantly, AhR is capable of modulating the responses of immune cells to environmental cues and endogenous signals from stromal or tumor cells [27-29]. Those exogenous signals contribute to the nuclear translocation and formation of AhR/ARNT heterodimers, thereby promoting the activation of downstream transcription factors [30]. Various experiments and clinical data have provided support for a potential link between AhR expression and tumor progression [31-33]. Upregulated AhR expression and transcriptional activity have been observed in serval tumor types, including breast, lung, and hepatocellular carcinoma [32, 34, 35]. And increasing evidence suggests that AhR activation promotes the migrative features of tumor cells and facilitates the establishment of drug resistance in breast cancer [36, 37]. Importantly, constitutive IDO expression correlated with AhR activation in human cancer, and the blockade of AhR activation by IDO/TDO signals restricts cancer immune suppression, reminding us of the potential role of AhR in IDO-TDO-associated tumor progression [38].

In this work, we further expanded the current understanding of tryptophan metabolism in tumor progression. Using TCGA/CCGA databases and clinical glioma tissues, we identified TDO2 as a pivotal driver that promoted glioma progression by enhancing tryptophan metabolism. Mechanistically, we demonstrated that TDO2 promoted the secretion of Kyn in glioma, which in turn helped activate pro-survival AhR/AKT signals in tumor cells and suppress anticancer responses of T cells. Blocking TDO signals efficiently suppressed glioma progression and improved chemotherapy outcome, pointing to a novel approach in glioma treatment.

Method and materials

Cell culture and reagents

LN229 and U87 cell lines were obtained from the Key Laboratory of Hubei Province for Digestive System Disease (Wuhan, Hubei, China) and cultured in DMEM (SH30023; HyClone) containing 10% fetal bovine serum (FBS, Gibico) at 37°C in a humidified atmosphere of 5% CO_2. For patient derived organoids, after informed consent, tumor samples classified as glioblastoma, based on the World Health Organization (WHO) criteria, were obtained from patients undergoing surgical treatment at the Affiliated Hospital of Southwest Medical University. Within 1-3 hours after surgical removal, tumors were washed in PBS and enzymatically dissociated into single cells. Tumor cells were cultured in NBE medium consisting of neurobasal medium (Thermo Fisher Scientific), N2 and B27 supplements (Thermo Fisher Scientific), and human recombinant bFGF and EGF (25 ng/mL each; R&D Systems) plus Heparin sodium and L-Glutamine.

Immunofluorescence

For immunofluorescence staining, LN229 or U87 were cultured in a six-well plate with cover glasses with different treatment, when cells were nearly full (80%), cover glasses were fixed with 4% paraformaldehyde for subsequent staining. Cell crawling cover glasses or glioma tissues sections from patients were incubated with 0.2% TritonX-100 (Beyotime) for 15 min and blocked in 3% BSA for 30 min. After washing by PBS for three times, the cells were incubated with primary antibodies against TDO2 (MAB9768; R&D system), SLC31A1 (ab133385; Abcam), AHR (GTX22770; GeneTex), IKK alpha (ab32041; Abcam), pAKT (#4060; Cell signaling technology), pCREB (#9198; Cell signaling technology), at 4°C overnight in wet chamber. On the following day, the slides were washed by PBST for three times and incubated with corresponding secondary antibodies at room temperature for 1 h. Nuclei was counterstained with 6-diamidino-2-phenylindole, dihy-

drochloride (DAPI, Thermo Fisher). Sections were mounted with the ProLong Gold Anti-fade Kit (Molecular Probes) and observed with a Nikon Eclipse Ti-U microscope equipped with a DS-Fi2 camera (Nikon). To determine the fluorescence signal in tissue sections, fluorescent-positive cells in five different high-power fields from each slide were quantified using ImageJ v1.50e (NIH) and presented as mean fluorescence intensity per square micrometer. Two to three slides from each sample were used for analysis.

Transfection, oligonucleotides and plasmids

The lentiviral vector plv-EF1a-TDO2-IRES-puro was constructed based on the backbone of the Plv-EF1a-IRES-puro (#85132; Addgene) vector. The EcoRI and BamHI restriction sites were used for the cloning. For TDO2 shRNA plasmids, the target sequences were cloned into a pLKO.1-puro vector obtained from ADDGENE according to the manufacturer's protocol. The following target sequences were used, sh1: 5'CCGGAGTGATAGGTACAAGGTATTTCTCGAGAAATACCTTGTACCTATCACTTTTTTTG3' and sh2: 5'CCGGGCACAAGAACTGCAAAGTGAACTCGAGTTCACTTTGCAGTTCTTGTGCTTTTTG3'. The DNA vectors were co-transfected into HEK293T cells with the helper plasmids psPAX2 and pMD2.G at a ratio of 10:5:2 for lentiviral packaging as described previously. Culture supernatant of 293T was used for infection of LN229 and U87.

Western blot analysis

Cells were collected and lysed in RIPA buffer (Byotime) containing Protease and Phosphatase Inhibitor Cocktails (Solarbio). Protein concentration was measured using a BCA Protein Assay kit (Solarbio). Aliquots of 30 μg protein samples were separated by electrophoresis on 10% SDS-polyacrylamide gels and then electrophoretically transferred to a methanol-pretreated PVDF membrane (Invitrogen). After blocking with 5% nonfat milk in TBST, the membrane was incubated with anti-TDO2 (ab76859; Abcam), anti-IKKα (ab32041; Abcam), anti-p-AKT (#4060, Cell signaling technology), and anti-β-actin antibodies. Blots were visualized with an HRP-conjugated secondary antibody (Byotime, China) and Western blotting analysis system (Tanon 4800, China). Relative protein expression was determined by ImageJ (NIH).

ELISA

The relative amounts of Kyn (Kyn ELISA Kit; Immundiagnostik AG), MMP2 (ab267813; Abcam) and MMP9 (ab246539; Abcam) in cell culture supernatants or tissue extraction were measured by ELISA according to the manufacturer's instructions. ELISA assay was based on an antibody sandwich method using microtiter plates. Briefly, a microplate pre-coated with capture antibody was provided and an HRP-labeled antibody (detection antibody, Streptavidin-HRP) was added and bound to the captured analyte. Tetramethylbenzidine (TMB) substrate solution was added to the wells and a blue color developed in proportion to the amount of analyte present in the sample. The optical density (O.D.) of each well was determined within 30 minutes using a microplate reader set to 450 nm and 570 nm. The standard curve was created by reducing the data using a computer software capable of generating a four-parameter logistic (4-PL) curve-fit.

Clone formation assay

LN229 and U87 cells treated in advance were seeded in six-well plates (300 cells per well) and cultured at 37°C for 13 days. Then, the cells were fixed with methyl alcohol for 10 min and stained with 4% crystal violet solution. The colonies in each group were washed before counting. ImageJ software (ImageJ 1.52a, United States) was used to analyze and quantify the number of colonies.

CCK-8 assay

In a 96-well plate, LN229 and U87 cells (2,000 cells per well) treated in advance were incubated with 10 μl per well Cell Counting Kit-8 (CCK-8, Biyuntian, Shanghai, China) reagent after 0, 24, 48, and 72 h, respectively. Cell proliferation rates were measured using a microplate reader (BD Biosciences, United States) to detect the absorbance at 450 nm.

Flowcytometry analysis

The following anti-human antibodies were used: APC anti-CD3 (HIT3a; Biolegend), PE anti-CD8 (SK1; Biolegend), Brilliant Violet 421 anti-PD-1 (EH12.2H7; Biolegend). Intranuclear staining was performed using the Fixation and Permeabilization Solution (554722; BD Bioscience)

according to the manufacturer's instructions and PE/Cyanine7 anti-IFNγ (4S.B3; Biolegend) and FITC anti-TNFα (MAb11; Biolegend) were used. When indicated, cytokine production was measured following 4 h in vitro stimulation with 50 mg/mL PMA, 500 mg/mL ionomycin and Monensin (475895; Sigma) was added to prevent excretion of the cytokines. LIVE/DEAD Fixable Violet Dead Cell Stain Kit (#L34955; Thermofisher) were used to exclude dead cells. Stained cells were analyzed on FACSCanto II and/or FACSARIA III systems and the data was analyzed with FlowJo version 9 or 10 software.

Cell migration assay

TDO2-OE or TDO2-sh LN229 and U87 cells treated either with or without Kyn, PDM2, MK-2206, IACS-8968 were resuspended in 200 μL medium without serum and were seeded into upper chambers of transwell chambers (Corning, USA) while lower chambers were filled with medium containing 10% FBS. To assess cell migration, the transwell migration assay was performed. Transfected cells were seeded in the top chambers containing 1% FBS, while medium containing 20% FBS was added to the lower chambers. After 24 h, the migrated cells on the bottom part of the membrane were fixed with 70% methanol and stained with 0.1% crystal violet. The cells from the top of the membrane were carefully removed, while the migrated cells were quantified in five random microscopic fields.

Animal experiment

Pathogen-free 6-week-old female Balb/c nude mice were obtained from SPF Biotechnology Co. Ltd. All animal experimental protocols were approved by the Ethics committee of the Affiliated Hospital of Southwest Medical University. Mice were bred in-house and fed on a standard animal chow diet. 2×10^5 TDO2-sh or TDO-OE LN229/U87 cells resuspended in 50 ul PBS were injected subcutaneously, tumor volume and survival are routinely recorded.

Analysis of TCGA and CGGA datasets

To explore the expression of TDO2 in cancer and patient survival, we analyzed TCGA and CGGA database. Kaplan-Meier survival curves were done based on two cohorts. GSEA method was used to analyze the relevant gene sets in the low expression group based on the CGGA cohort.

Statistical analysis

Concentrations of tryptophan metabolites were normalized to cecal or fecal wet weight. All data were compared using either Student's t test, one-way or two-way analysis of variance with Tukey multiple comparison posttest, where appropriate, in GraphPad Prism 8 (GraphPad Software, Inc, La Jolla, CA, USA) to determine statistical significance between different groups. The value of $P<.05$ was considered statistically significant (*P<.05; **P<.01; ***P<.001; ****P<.0001).

Results

TDO-associated tryptophan metabolism promoted tumor progression in glioma patients

To identify glioma gene expression signatures, analysis of gene expression in glioma tissues based on the rich set of CCGA database was performed. Glioma tissues from 325 patients were divided into the high degree group (H-D, WHO level 1~2) and low degree group (L-D, WHO level 3~4). Intriguingly, we found a high rate of tryptophan metabolism-associated genes that were up-regulated in high-degree glioma tissues, including the tryptophan transporter SLC31A1 and tryptophan 2,3-dioxygenase 2 (TDO2) (**Figure 1A**). To better understand the signaling pathway signatures in high-degree glioma development, KEGG pathway analysis was performed in 325 tumor tissues from high-degree glioma patients. Consistently, strengthened tryptophan metabolism-associated signaling pathways were observed in those glioma tissues (**Figure 1B**), suggesting a potential correlation between tryptophan metabolism and glioma development. TDO2, a tryptophan metabolism-associated enzyme, is able to cleave indoleamine derivatives such as tryptamine and serotonin. We further collected tumor tissues from glioma patients to examine the expression TDO2. Higher expression of TDO2 was observed in tumor tissues from high-degree glioma patients (**Figure 1C**). Both CCGA and TCGA databases also revealed poor overall survival rates in patients with high TDO2 expression compared to the TDO2 low group (**Figure 1D** and **1E**). These results implied that enhanced tryptophan metabolism induced by

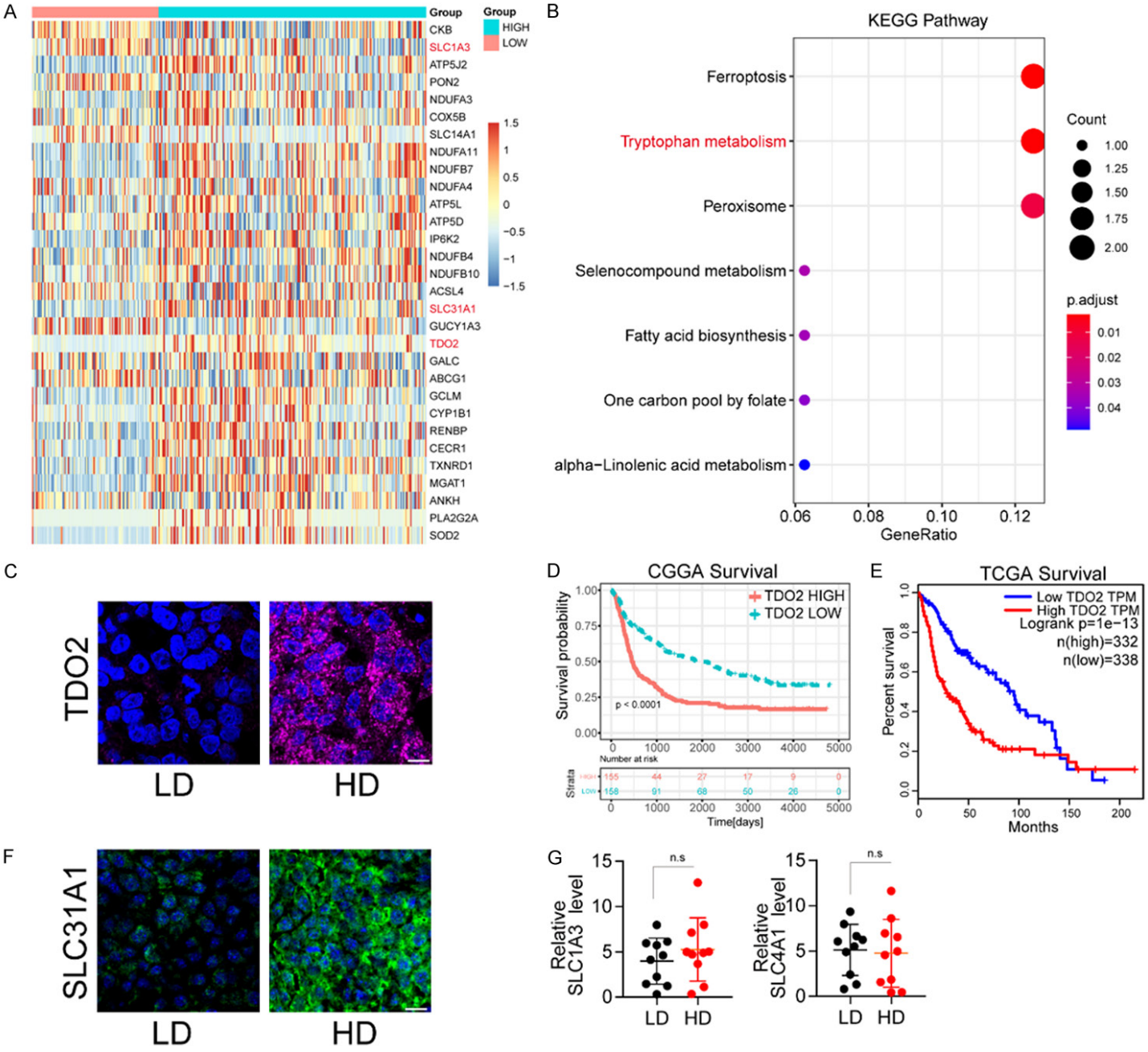
A
Group
Group
HIGH
LOW
CKB
SLC1A3
ATP5J2
PON2
NDUFA3
COX5B
SLC14A1
NDUFA11
NDUFB7
NDUFA4
ATP5L
ATP5D
IP6K2
NDUFB4
NDUFB10
ACSL4
SLC31A1
GUCY1A3
TDO2
GALC
ABCG1
GCLM
CYP1B1
RENBP
CECR1
TXNRD1
MGAT1
ANKH
PLA2G2A
SOD2
1.5
1
0.5
0
−0.5
−1
−1.5
B
KEGG Pathway
Ferroptosis
Tryptophan metabolism
Peroxisome
Selenocompound metabolism
Fatty acid biosynthesis
One carbon pool by folate
alpha−Linolenic acid metabolism
0.06
0.08
0.10
0.12
GeneRatio
Count
1.00
1.25
1.50
1.75
2.00
p.adjust
0.01
0.02
0.03
0.04
C
TDO2
LD
HD
D
CGGA Survival
TDO2 HIGH
TDO2 LOW
Survival probability
1.00
0.75
0.50
0.25
0.00
p < 0.0001
0
1000
2000
3000
4000
5000
Number at risk
Strata
HIGH 155 44 27 17 9 0
LOW 158 91 68 50 26 0
Time[days]
E
TCGA Survival
Low TDO2 TPM
High TDO2 TPM
Logrank p=1e−13
n(high)=332
n(low)=338
Percent survival
0.0
0.2
0.4
0.6
0.8
1.0
0
50
100
150
200
Months
F
SLC31A1
LD
HD
G
n.s
Relative SLC1A3 level
15
10
5
0
LD
HD
n.s
Relative SLC4A1 level
15
10
5
0
LD
HD

Figure 1. TDO associated tryptophan metabolism promoted tumor progression in glioma patients. A. Heatmap of metabolism associated gene based on the CGGA cohort. B. KEGG analysis of all of the pathways in the High degree glioma. C. Immunofluorescence analysis of TDO2 in low degree (LD) malignancy and high degree (HD) malignancy glioma tissues from patients. Bar=50 μm. D. Kaplan-Meier analysis of the TDO2 expression based on the CGGA cohort. E. Kaplan-Meier analysis of the TDO2 expression based on the TGGA cohort. F. Immunofluorescence analysis of SLC31A1 in LD and HD glioma tissues from patients. Bar=50 μm. G. ELISA analysis for the secretion of SLC1A3 and SLC4A1 level in tumor cell from LD and HD glioma tissues from patients. Means ± SEM of three independent experiments. *P<0.05, **P<0.01.

TDO2 might be correlated to the tumor progression and poor prognosis in glioma patients. Next, we further examined the expression of tryptophan transporters in tumor tissues from glioma patients. Elevated expression of the tryptophan transporter SLC31A1 was observed in high-degree glioma tissues (**Figure 1F**), whereas no significant difference was observed for SLC1A3 or SLC14A1 (**Figure 1G**), suggesting that tryptophan transport was dependent on the expression of SLC31A1 rather than SLC1A3 or SLC4A1 in glioma. Together, those results suggested that the TDO2-associated tryptophan metabolism process might promote tumor progression in glioma.

Suppression of TDO-associated tryptophan metabolism retarded glioma progression

To further validate the role of tryptophan metabolism and TDO2 in glioma, we overexpressed TDO2 in glioma cell lines LN229 and U87 (**Figure 2A**). We found that TDO2 overexpression significantly promoted the proliferation of LN229 and U87 cells *in vitro* (**Figure 2B**) and tumor growth i*n vivo* (**Figure 2C**). Next, we knocked down (KO) the expression of TDO2 in LN229 and U87 cells (**Figure 2D**). Blocking TDO2-dependent tryptophan metabolism clearly suppressed cell proliferation of U87 and LN229 *in vitro* (**Figure 2E**) and *in vivo* (**Figure 2F**). To further identify the role of TDO2 in tryptophan metabolism, we maintained glioma cells in tryptophan-free culture medium. Intriguingly, tryptophan deficiency reversed the protumor effects induced by TDO2 in glioma cells and no significant difference in cell proliferation was observed in TDO2 overexpression or KO LN229/U87 cells (**Figure 2G**), indicating that TDO2-induced tryptophan metabolism facilitated glioma cell proliferation and tumor growth. Next, we examined the colony formation and cell invasion capabilities of TDO2 overexpression/KO glioma cells. Consistently, TDO2 overexpression promoted colony formation while TDO2 KO suppressed colony formation in LN229 and U87 cells (**Figure 2H**, **2I**). Similar results were observed in our transwell analysis (**Figure 2J**, **2K**), indicating that aberrant tryptophan metabolism induced by TDO2 could facilitate glioma tumor invasion and tumorigenesis. Together with our previous results, these findings suggest that TDO2-induced tryptophan metabolism could promote glioma progression.

Kyn derived from tryptophan metabolism mediated glioma growth through an autocrine pathway

Next, we sought to determine the downstream signaling pathway in tryptophan/TDO2-induced tumor progression. We added four tryptophan metabolites, including melatonin, kynurenic acid, indoxyl sulfate, and Kyn, into the culture medium of glioma cells. Notably, Kyn treatment significantly promoted LN229 and U87 cell proliferation, whereas no difference was observed in the melatonin, kynurenic acid, and indoxyl sulfate treatment groups (**Figure 3A**). To identify the pro-tumor effects of Kyn, we examined the expression of Kyn in tumor tissues from glioma patients. And increased Kyn secretion was found in tumor tissues from high-degree glioma patients (**Figure 3B**). More importantly, enhanced Kyn secretion was observed in TDO2 overexpression LN229/U87 cells while suppression of TDO2 retarded Kyn expression (**Figure 3C**, **3D**), indicating that TDO2 promoted tryptophan metabolism to produce Kyn, thereby resulting in glioma development. To confirm our hypothesis, we treated TDO2 KO LN229/U87 cells with Kyn, which efficiently promoted the proliferation of TDO2 KO glioma cells (**Figure 3E**). Consistently, injecting Kyn to TDO2 KO LN229/U87-bearing mice promoted tumor growth *in vivo* (**Figure 3F**). Next, we added Kyn into the culture medium for colony formation analysis of TDO2 KO LN229/U87 cells. As anticipated, enhanced colony formation capability was observed in LN229/U87 KO cells treated with Kyn (**Figure 3G**). Kyn treatment also facilitated cell invasion of these cells (**Figure 3H**). Together, those results implied that TDO2 pro-

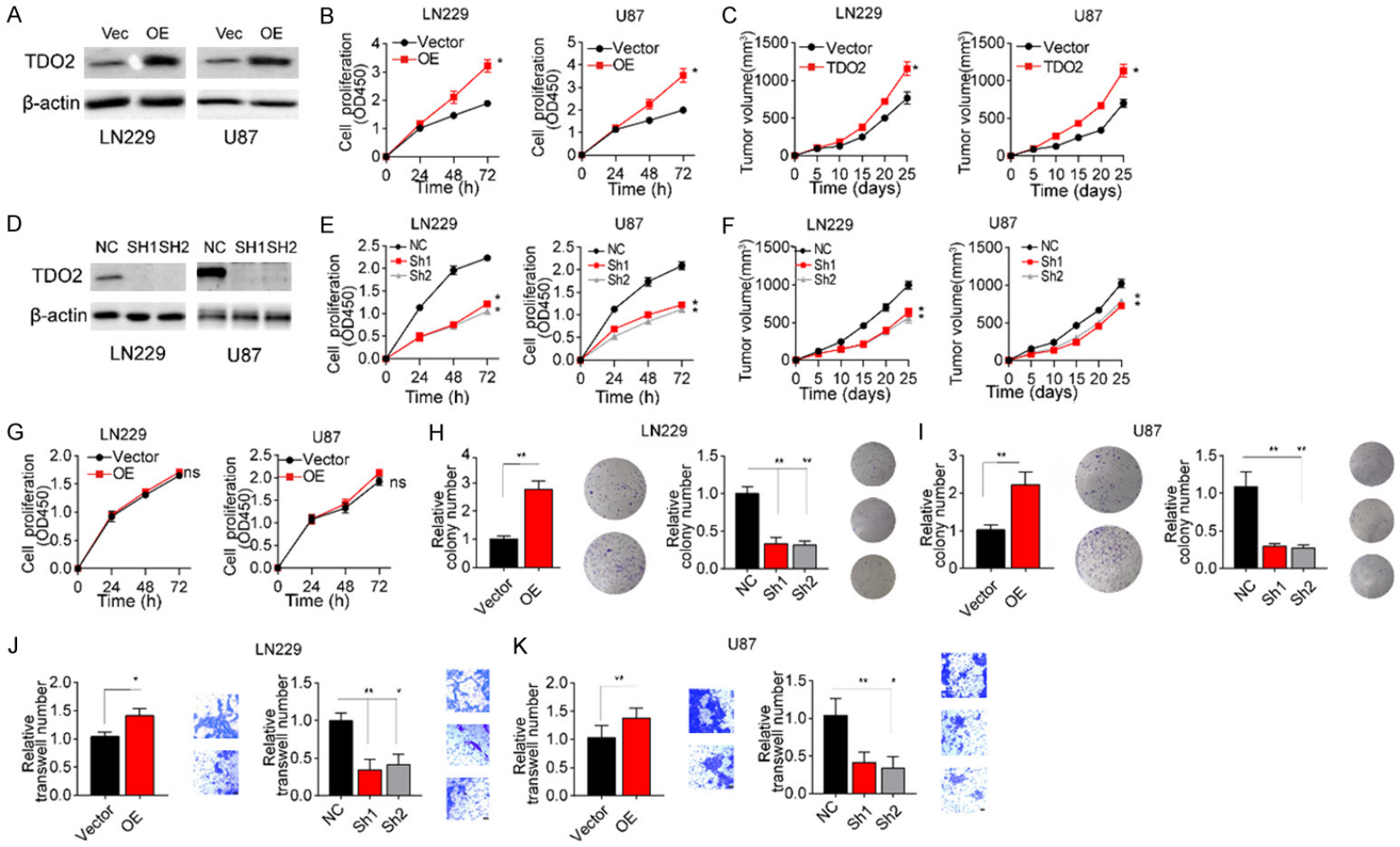

Figure 2. Suppression of TDO associated Trp metabolism retarded glioma progression. A. Western analysis of cellular levels of TDO2 overexpression in the LN229 and U87 cells. B. The cell proliferation of LN229-Vector, LN229-TDO2 overexpression, U87-Vector and U87-TDO2 overexpression cells. C. Tumor volume was measured at various time points of LN229-Vector, LN229-TDO2 overexpression, U87-Vector and U87-TDO2 overexpression bearing mice. D. Western analysis of cellular levels of TDO2 silence in the LN229 and U87 cells. E. The cell proliferation of LN229-NC, LN229-SH1, U87-SH2 cell lines (Left), the cell proliferation of U87-NC, U87-SH1, U87-SH2 cell lines (Right). F. Tumor volume was measured at various time points of LN229-NC, LN229-SH1 and LN229-SH2 bearing mice (Left), Tumor volume was measured at various time points of U87-NC, U87-SH1 and U87-SH2 bearing mice (Right). G. The cell proliferation of LN229-Vector, LN229-TDO2 overexpression, U87-Vector and U87-TDO2 overexpression cells cultured in free Trp. H. Colony formation analysis of LN229-Vector and LN229-TDO2 overexpression cells (Left), Colony formation analysis of LN229-NC, LN229-SH1 and LN229-SH2 cells (Right). I. Colony formation analysis of U87-Vector and U87-TDO2 overexpression cells (Left), Colony formation analysis of U87-NC, U87-SH1 and U87-SH2 cells (Right). J. Relative numbers of invasive LN229-Vector and LN229-TDO2 overexpres-

sion cells, Relative numbers of invasive LN229-NC, LN229-SH1 and LN229-SH2 cells. Bar=25 μm. K. Relative numbers of invasive U87-Vector and U87-TDO2 overexpression cells, Relative numbers of invasive of U87-NC, U87-SH1 and U87-SH2 cells. Bar=25 μm. Means ± SEM of three independent experiments. NC, shBFP, *P<0.05, **P<0.01.

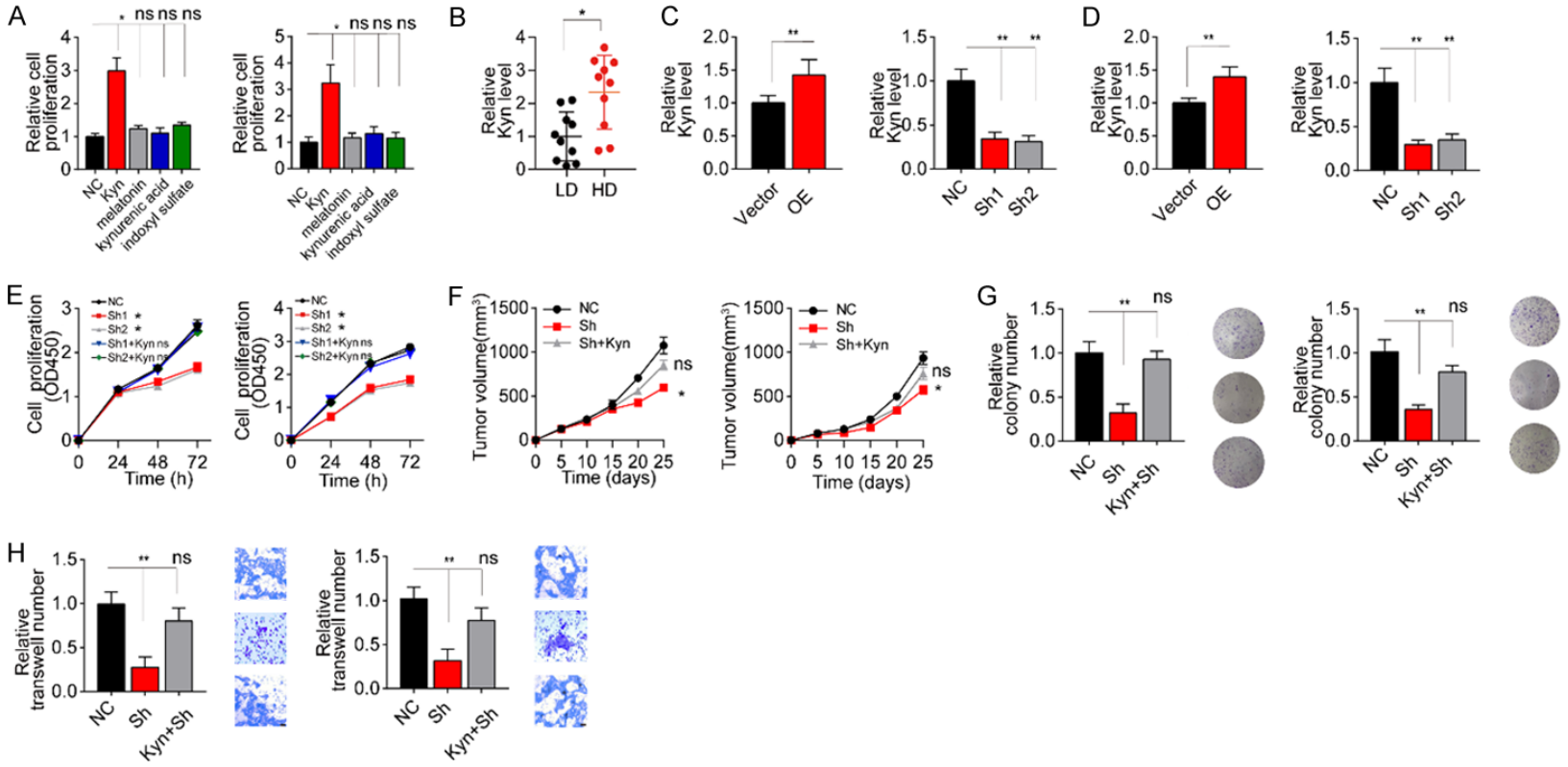

Figure 3. Kyn derived from Trp metabolism mediated glioma growth through an autocrine pathway. A. The cell proliferation of LN229 or U87 cells treated with PBS, melatonin (100 μM), kynurenic acid (100 μM), indoxyl sulfate (100 μM) and Kyn (100 μM) at 72 hours. B. ELISA analysis for the secretion of Kyn level in tumor cell from LD and HD glioma tissues from patients. C. ELISA analysis for the secretion of Kyn level in LN229-Vector and LN229-overexpression cells, ELISA analysis for the secretion of Kyn level in LN229-NC, LN229-SH1 and LN229-SH2 cells. D. ELISA analysis for the secretion of Kyn level in U87-Vector and U87-overexpression cells, ELISA analysis for the secretion of Kyn level in U87-NC, U87-SH1 and U87-SH2 cells. E. The cell proliferation of LN229-NC, LN229-SH1, LN229-SH2 treated with PBS or Kyn (100 μM) for different time (Left). The cell proliferation of U87-NC, U87-SH1, U87-SH2 treated with PBS or Kyn (100 μM) for different time (Right). F. Tumor volume was measured at various time points of LN229-NC, LN229-SH bearing mice treated with PBS or Kyn (Left), Tumor volume was measured at various time points of U87-NC, U87-SH and U87-SH bearing mice treated with PBS or Kyn (Right). G. Colony formation analysis of LN229-NC and LN229-SH, LN229-SH treated with Kyn (100 μM) (Left), the colony formation analysis of U87-NC and U87-SH, U87-SH treated with Kyn (100 μM) (Right). H. Relative numbers of invasive LN229-NC, LN229-SH and LN229-SH cells treated with Kyn (100 μM) (Left), relative numbers of invasive U87-NC and U87-SH, U87-SH cells treated with Kyn (100 μM) (Right). Bar=25 μm. Means ± SEM of three independent experiments. NC, DMSO, *P<0.05, **P<0.01.

moted glioma progression through Kyn derived from tryptophan metabolism.

Kyn facilitated glioma development through an AhR/AKT pathway

Kyn has been reported previously to act as an oncometabolite through up-regulating AhR signals that target AKT pathways [38]. Therefore, we determined whether Kyn could promote the activation of AhR and AKT signals in glioma cells. Here, enhanced AhR expression was observed in LN229/U87 cells treated with Kyn (**Figure 4A**). And our gene set enrichment analysis based on 325 glioma patients revealed a high correlation between the AKT signaling pathway and glioma development (**Figure 4B**). We further examined the expression of iKK α and AKT in glioma cells treated with Kyn. Consistently, Kyn treatment facilitated the expression of phosphorylated iKK α and AKT, whereas inhibition of AhR by the inhibitor PDM2 suppressed iKK α/AKT up-regulation induced by Kyn (**Figure 4C**), indicating that Kyn mediated AKT signaling activation through AhR signals. To further validate the role of AhR/AKT signals in glioma progression, we used the AhR inhibitor PDM2 and AKT inhibitor MK2206 to treat glioma cells. Notably, PDM2 or MK2206 treatment significantly suppressed the Kyn-induced proliferation of LN229 and U87 cells (**Figure 4D**). Blocking AhR/AKT signals also suppressed Kyn-induced colony formation (**Figure 4E**) and cell invasion (**Figure 4F**), suggesting that Kyn facilitated glioma development through an AhR/AKT-dependent signaling pathway. Next, we further examined the expression of AhR and phosphorylated AKT in glioma patients. Again, elevated expression of AhR and phosphorylated AKT was observed in tumor tissues from high-degree glioma patients (**Figure 4G**). More importantly, both AhR (**Figure 4H**) and phosphorylated AKT (**Figure 4I**) showed high correlation to Kyn expression in glioma tissues (AhR and Kyn R^2=0.45, AKT and Kyn R^2=0.43). Together, these results suggested that Kyn produced from tryptophan metabolism promoted glioma development through AhR/AKT signals.

Kyn promoted glioma invasion through the AKT/CREB-dependent EMT process

Next, we wondered how Kyn promoted tumor cell invasion in glioma. CREB serves as a downstream molecule of AKT and participates in the tumor metastasis and invasion process in several tumor types. Herein, we examined the expression of CREB in Kyn-treated glioma cells. Elevated expression of phosphorylated CREB was found in Kyn-treated LN229 and U87 cells, whereas suppression of AhR or AKT retarded the up-regulation of phosphorylated CREB (**Figure 5A**). More importantly, gene set enrichment analysis revealed that the EMT process exhibited a high correlation with glioma progression (**Figure 5B**). Thus, we speculated that AhR/AKT signaling might be involved in glioma cell invasion through a CREB-dependent EMT process. Thus, we examined the expression of E-cadherin (a marker of epithelial-like cells) and N-cadherin (a marker of mesenchymal-like cells) in LN229/U87 cells. Intriguingly, Kyn treatment significantly up-regulated N-cadherin but down-regulated E-cadherin expression in U87 and LN229 cells, whereas the CREB inhibitor 666-15 suppressed the EMT process induced by Kyn (**Figure 5C**). Consistently, Kyn treatment also promoted the expression of Snail and Slug (**Figure 5D**), as well as MMP2 and MMP9 (**Figure 5E** and **5F**). Meanwhile, CREB inhibition retarded the up-regulation of pro-invasion factors (**Figure 5E** and **5F**). Similar results were observed at the mRNA level (Figure S1A) and *in vivo* (Figure S1B and 1C), suggesting that Kyn mediated EMT through AhR/AKT/CREB signals, resulting in the up-regulation of Snail/Slug/MMP2/MMP9 and tumor invasion. We further examined the expression of CREB in tumor tissues from patients and found high levels of phosphorylated CREB in high-degree glioma tissues, especially in stage IV glioma tissues (**Figure 5G**). High expression of MMP2 and MMP9 was also observed in stage IV glioma tissues (**Figure 5H**).

Glioma cells mediated immunosuppression through Kyn secretion

We have demonstrated that Kyn could mediate the activation of AKT pro-survival signaling pathway to regulate tumor progression in glioma. However, some tumor tissues still revealed rapid tumor growth (stage III or IV), but showed no significant activation of AKT signals despite of high Kyn or TDO expression (**Figure 4H**). The low expression of AKT might be due to deficiencies or mutations of signaling molecules upstream of AKT. However, we wondered about the underlying mechanism of tumor progres-

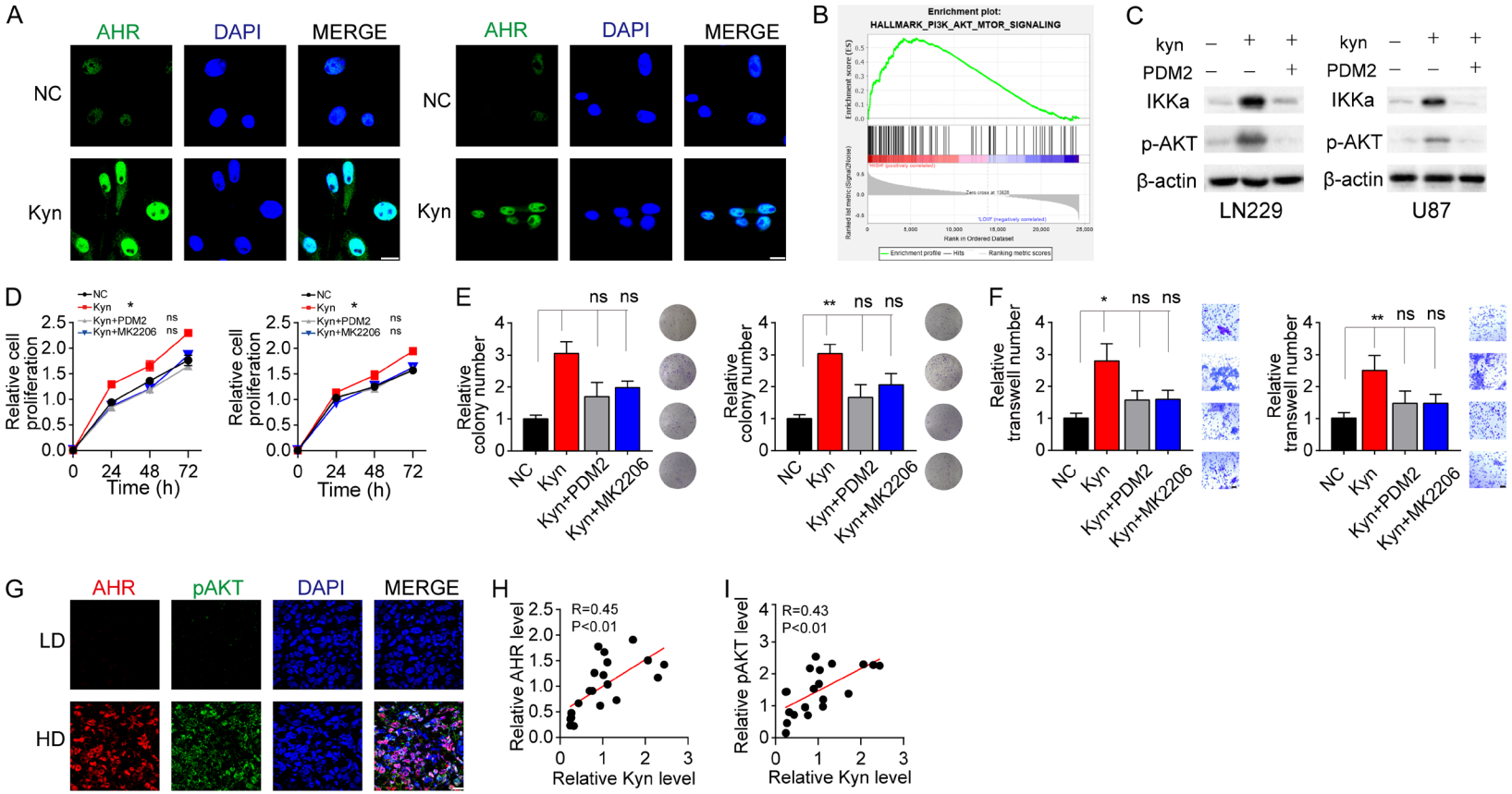

Figure 4. Kyn facilitated glioma development through an AhR/AKT pathway. (A) Immunofluorescence analysis of AhR in LN229 (Left) or U87 (Right) cells treated with DMSO or Kyn (100 μM). Bar=25 μm. (B) Gene set enrichment analysis (GSEA): The "PI3K-AKT" gene set was enriched in the SET low expression group based on the CGGA dataset. (C) Western blotting assay of iKK α and AKT expression in LN229 and U87 cells treated with DMSO, Kyn (100 μM) or combination with Kyn and PDM2 (50 μM). (D) The cell proliferation of LN229 or U87 treated with DMSO, Kyn, Kyn combined with PDM2 (50 μM) or Kyn (100 μM) combined with MK2206 (5 μM). (E) Colony formation analysis of LN229 or U87 treated with DMSO, Kyn (100 μM), Kyn (100 μM) combined with PDM2 (50 μm) or Kyn (100 μM) combined with MK2206 (5 μM). (F) Relative numbers of invasive LN229 or U87 cells treated with DMSO, Kyn (100 μM), Kyn (100 μM) combined with PDM2 (50 μM) or Kyn (100 μM) combined with MK2206 (5 μM). (G) Immunofluorescence analysis of AhR and p-AKT in LD and HD glioma tissues from patients. Bar=50 μm. (H, I) Correlation study between p-AKT (H) and Kyn (I) in LD and HD glioma tissues from patients. Means ± SEM of three independent experiments. NC, DMSO, *P<0.05, **P<0.01.

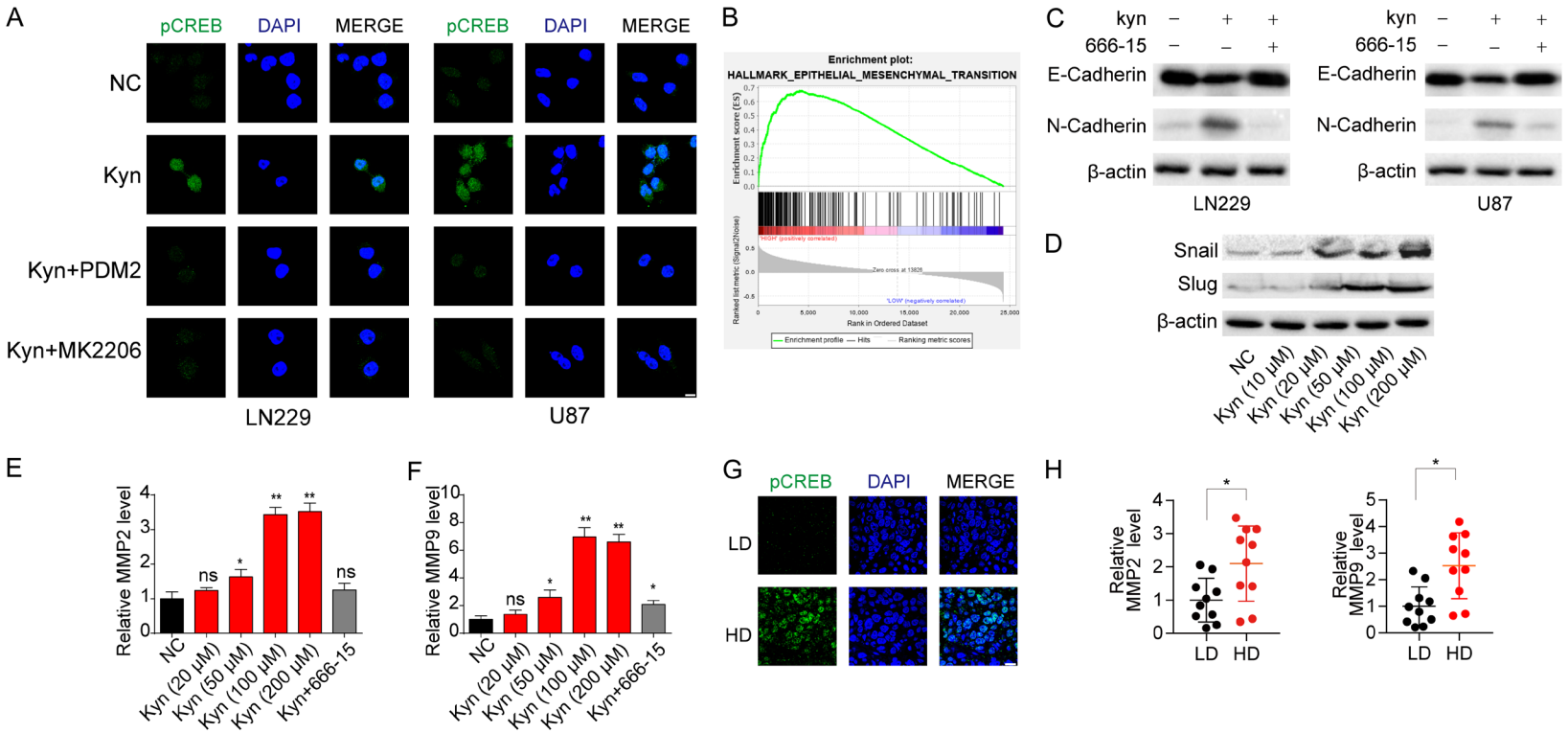

Figure 5. Kyn promoted glioma invasion through AKT/CREB dependent EMT process. A. Immunofluorescence analysis of p-CREB in LN229 (Left) or U87 (Right) cells treated with DMSO, Kyn (100 μM), Kyn (100 μM) combined with PDM2 (50 μM) or Kyn (100 μM) combined with MK2206 (5 μM). Bar=25 μm. B. Gene set enrichment analysis (GSEA): The "EMT" gene set was enriched in the SET low expression group based on the CGGA dataset. C. Western blotting assay of E-cadherin and N-cadherin expression in LN229 and U87 cells treated with DMSO, Kyn (100 μM), Kyn (100 μM) combined with 666-15 (100 μM). D. Western blotting assay of Snail and Slug in LN229 cells treated with NC or Kyn (10 μM), Kyn (20 μM), Kyn (50 μM), Kyn (100 μM) and Kyn (200 μM). E and F. ELISA analysis for the secretion of MMP2 and MMP9 level in LN229 cells treated with DMSO, Kyn (20~200 μM) or Kyn (100 μM) combined with 666-15 (1 μM). G. Immunofluorescence analysis of p-CREB in LD and HD glioma tissues from patients. Bar=50 μm. H. ELISA for the secretion of MMP2 and MMP9 level in tumor cell from LD and HD glioma tissues from patients. Means ± SEM of three independent experiments. NC, DMSO, *P<0.05, **P<0.01.

sion in the absence of AKT. Tumor progression involves diverse biological processes, including pro-survival signaling pathway activation of tumor cells and immunosuppression in the tumor microenvironment. Here, we found decreased T cell distribution, including total T cells (**Figure 6A**) and cytotoxic CD8-positive T cells (**Figure 6B**), in high-degree glioma tissues with low expression of AKT compared to high-degree glioma tissues with high AKT expression. More importantly, cytotoxic CD8-positive T cells isolated from those glioma tissues revealed low expression of IFN-γ and TNF-α (**Figure 6C**) compared to T cells isolated from high-degree glioma tissues with AKT expression, reminding us of immunosuppression in those high-degree glioma tissues. Next, we further investigated the underlying mechanism of T cell suppression. We isolated naïve T cells from mouse spleens using CD3 magnetic cell sorting and used concanavalin A to induce T cell activation. Subsequently, we treated those T cells with Kyn. Notably, the proliferation of T cells (total and cytotoxic CD8-positive T cells) was suppressed by Kyn treatment (**Figure 6D** and **6E**). More importantly, the secretion of IFN-γ and TNF-α (**Figure 6F**) by cytotoxic CD8-positive T cells in the Kyn-treated group was reduced compared to the DMSO group, indicating that Kyn suppressed T cell proliferation and activation. Additionally, higher PD-1 expression was observed in CD8 T cells treated with Kyn (**Figure 6G**). Similar results were observed in T cells from tumor tissues from high-degree glioma (**Figure 6H**), suggesting that Kyn could suppress T cell activation through up-regulating PD-1 expression. Together, the above results suggested Kyn derived from tumor cells could further regulate glioma progression through T cell suppression.

The blockade of TDO signals improved the tumor suppressive effects of chemotherapy

Given the curial role of Kyn in regulating glioma progression, we reasoned that it might be feasible to suppress the Kyn upstream molecule TDO2 to retard tumor growth. Herein, we combined the IDO/TDO inhibitor IACS-8968 with chemotherapy. Co-treatment with IACS-8968 significantly strengthened the cytotoxicity of TMZ in glioma cells (**Figure 7A**), especially TDO2 overexpression LN229 and U87 cells (**Figure 7B**). More importantly, blocking TDO2 signals also suppressed the colony formation (**Figure 7C**) and invasion capabilities (**Figure 7D**) of LN229 and U87 cells. Next, we further established LN229 and U87 subcutaneous bearing mice, then treated these mice with PBS, IACS-8968, TMZ, or TMZ combined with IACS-8968. Consistently, the combination of TMZ and IACS-8968 revealed superior anticancer effects (**Figure 7E** and **7F**) and efficiently prolonged the survival of tumor-bearing mice (**Figure 7G** and **7H**). In order to further confirm the anticancer effects of IACS-8968 in clinical glioma treatment, we isolated glioma cells from six high-degree (stage III~IV) and low-degree patients (stage I~II) and seeded the cells into 3D matrix gels for *in vitro* cell cytotoxicity analysis. Glioma cells from two patients showed proliferative characteristics with spherical colony formation (**Figure 7I**). Consistent with our results above, glioma cells cultured in 3D fibrin gels revealed high expression of TDO2 (**Figure 7J**) as well as activation of AhR/AKT/CREB signals (**Figure 7J**). Subsequently, we added IACS-8968 and TMZ into the 3D culture system for cytotoxicity analysis. As anticipated, cell apoptosis was apparent in the IACS-8968/TMZ combination group, indicating strengthened tumor suppressive effects of IACS-8968 and TMZ on patient-derived glioma cells. Together, those results suggested that blockade of TDO2 signals by IACS-8968 could efficiently improve the anticancer effects of chemotherapy and represent a novel strategy for glioma treatment.

Discussion

In this study, we showed for the first time that tryptophan metabolism driven by TDO2 was associated with detrimental tumor progression and poor prognosis in glioma patients. Tumor cells with high levels of tryptophan metabolizing dioxygenases IDO/TDO exhibited up-regulated signaling pathways involved in tumor growth, DNA repair and distant metastasis. In accordance with previous studies that found decreased tryptophan and increased Kyn level in the serum to correlate with tumor progression, we further linked the tryptophan metabolite Kyn to glioma development and demonstrated that autocrine Kyn induced by TDO2 could facilitate glioma cell proliferation and invasion. Using TCGA/CCGA databases and clinical glioma tissues, we also found that the

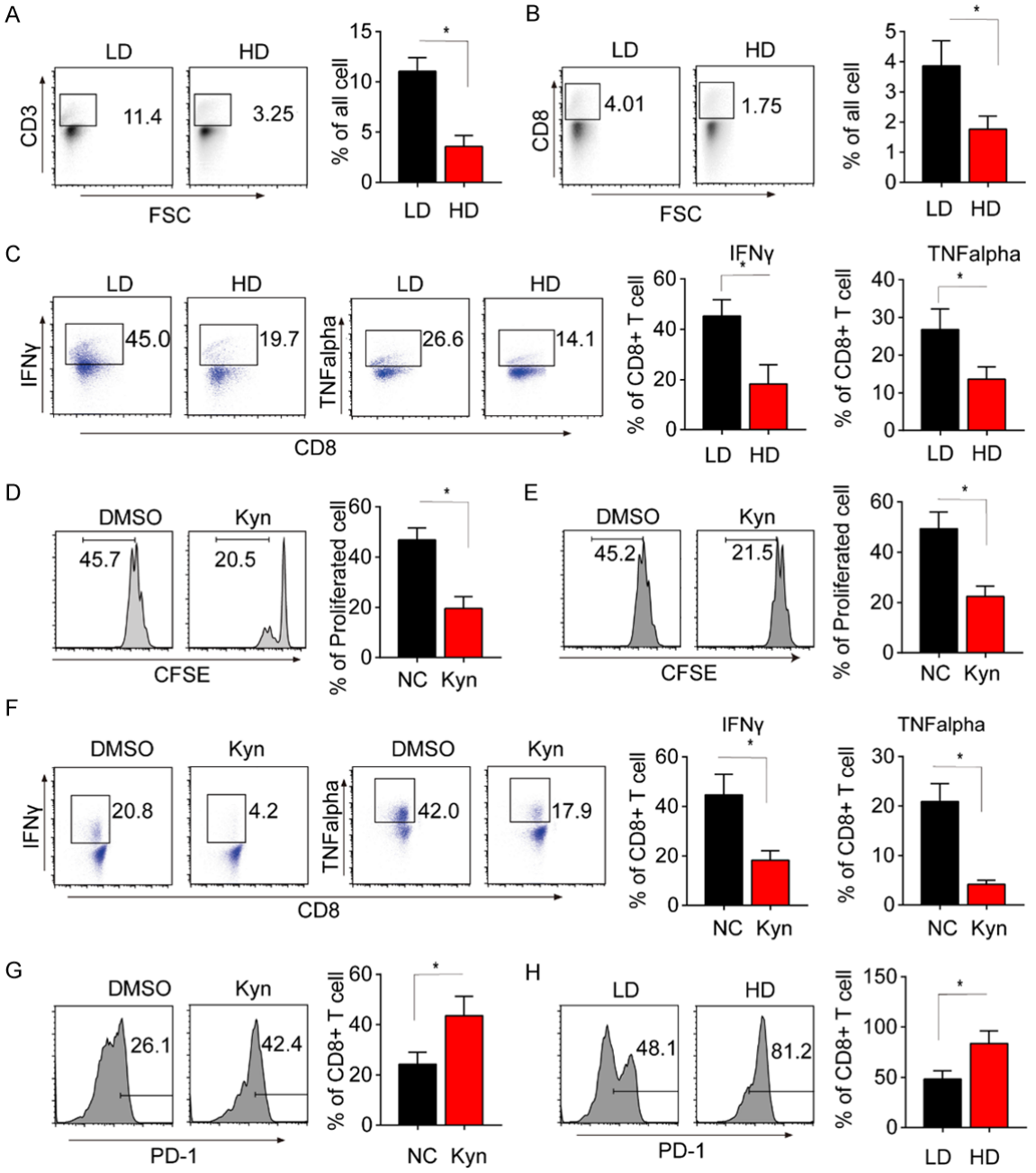

Figure 6. Glioma cells mediated immunosuppression through Kyn secretion. A. Flow cytometric plot of the percentage of $CD3^+$ cell in tumor cell from LD and HD glioma tissues from patients (Left). Flow cytometric quantification of the percentage of $CD3^+$ cell (Right). B. Flow cytometric plot of the percentage of $CD8^+$ cell in tumor cell from LD and HD glioma tissues from patients (Left). Flow cytometric quantification of the percentage of $CD8^+$ T cell (Right). C. Representative flow cytometric plots of human $CD8^+$ T cells examined for the expression of IFN-γ and TNF-α in tumor cell from LD and HD glioma tissues from patients (Left). The percentage of IFN-γ or TNF-α in $CD8^+$ T cells (Right). D. Representative histogram of CFSE-labeled spleen of mice total T cells (stimulated with anti-CD3/CD28 antibodies) after treatment with DMSO or Kyn (100 μM) (Left). The proportion of cells with diluted CFSE dye (Right). E. Representative histogram of CFSE-labeled of mice $CD8^+$ T cells (stimulated with anti-CD3/CD28 antibodies) after treatment with DMSO or Kyn (100 μM) (Left). The proportion of cells with diluted CFSE dye (Right). F. Representative flow cytometric plot of mice $CD8^+$ T cells treated with DMSO or Kyn (100 μM) examined for the expression of IFN-γ and TNF-α (Left). Flow cytometric quantification of the percentage of IFN-γ or TNF-α in $CD8^+$ T cells (Right). G. Representative flow cytometric histograms of $CD8^+$ T cells treated with DMSO or Kyn (100 μM) examined for the expression of PD-1 (Left). H. Representative flow cytometric histograms of $CD8^+$ T cells in tumor cell from LD and HD glioma tissues from patients examined for the expression of PD-1, Flow cytometric quantification of the percentage of PD-1 cell (Right). Means ± SEM of three independent experiments. NC, DMSO, *P<0.05, **P<0.01.

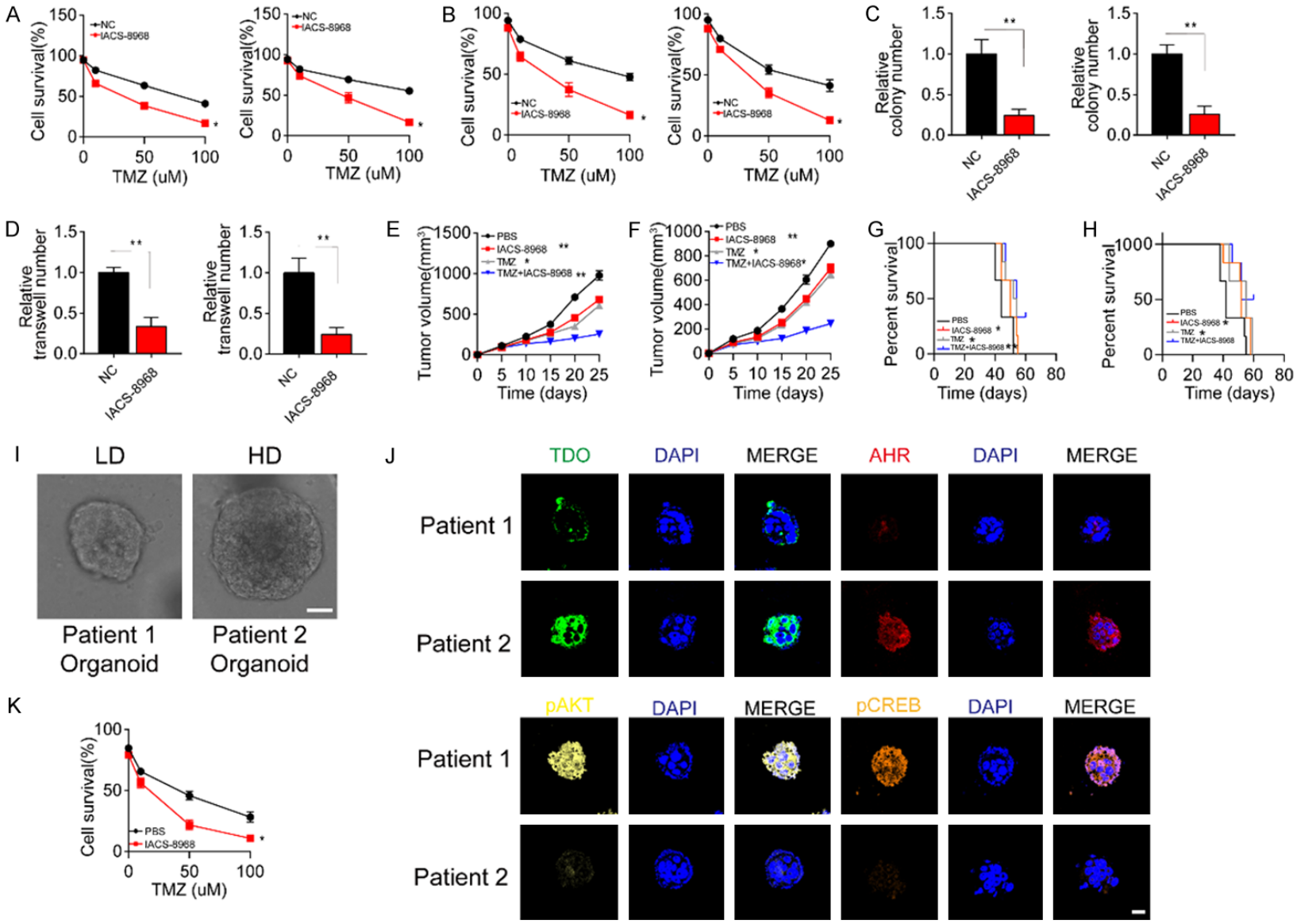
A
Cell survival(%)
NC
IACS-8968
TMZ (uM)
B
C
Relative colony number
D
Relative transwell number
E
Tumor volume(mm3)
PBS
IACS-8968
TMZ
TMZ+IACS-8968
Time (days)
F
G
Percent survival
H
I
LD
HD
Patient 1 Organoid
Patient 2 Organoid
J
TDO
DAPI
MERGE
AHR
Patient 1
Patient 2
pAKT
pCREB
K

Figure 7. Blockade of TDO signals improved tumor suppressive effects of chemotherapy. A. Relative cell cytotoxicity of LN229 and U87 cells treated with TMZ (200 μM) or TMZ (200 μM) combined with IACS-8968 (10 μM) determined by cells apoptosis analysis. B. Relative cell cytotoxicity of LN229 TDO2 overexpression and U87 TDO2 overexpression cells treated with TMZ (200 μM) or TMZ combined with IACS-8968 determined by cells apoptosis analysis. C. Colony formation analysis of LN229 cells treated with DMSO or IACS-8968 (Left), colony formation analysis of U87 cells treated with DMSO or IACS-8968 (Right). D. Relative numbers of invasive LN229 cells treated with DMSO or IACS-8968 (Left), relative numbers of invasive U87-cell treated with DMSO or IACS-8968 (Right). E. Tumor volume was measured at various time points of LN229 bearing mice treated with DMSO, IACS-8968 (5 mg/kg), TMZ (10 mg/kg), TMZ (10 mg/kg) combined with IACS-8968. F. Tumor volume was measured at various time points of U87 bearing mice treated with DMSO, IACS-8968, TMZ (10 mg/kg), TMZ (10 mg/kg) combined with IACS-8968 (5 mg/kg) on bearing mice. G. Survival time of LN229 cell-bearing mice treated with DMSO, IACS-8968, TMZ (10 mg/kg), TMZ (10 mg/kg) combined with IACS-8968. H. Survival time of U87 cell-bearing mice treated with DMSO, IACS-8968, TMZ (10 mg/kg), TMZ (10 mg/kg) combined with IACS-8968. I. Organoid cultures from LD and HD glioma tissues from patients were established. Depicted are representative organoids at day 4. Bar=25 μm. J. Immunofluorescence analysis of TDO2, AhR/pAKT/pCREB expression in organoid derived LD and HD glioma tissues from patient. Bar=25 μm. K. Relative cell cytotoxicity of glioma cells treated with TMZ (200 μM) or TMZ (200 μM) combined with IACS-8968 (10 μM) determined by cells apoptosis analysis. The data are presented as means ± SEM of three independent experiments. NC, DMSO, *P<0.05, **P<0.01.

expression of TDO2 revealed a high correlation with the prognosis in glioma patients, indicating that the level of TDO2 expression could serve as an important indicator of glioma progression.

Plasma tryptophan status and the tryptophan/Kyn ratio are influenced by both tryptophan-degrading enzymes IDO1 and TDO2 [18, 22, 39]. The expression of IDO1 has been recognized as having a crucial role in promoting tumor progression and immunosuppression in the microenvironment, in which the immune inhibitory metabolites induced by IDO1 can repress functional T cell proliferation and facilitate T cell apoptosis [40, 41]. Consistently, reduction in $CD3^+$ and $CD8^+$ T cells was found in our glioma samples with TDO2 expression. Meanwhile, the secretion of IFN-γ and TNF-α was repressed in those T cells. In those glioma tissues, Kyn derived from tumor cells was implicated in the direct inhibitory effects of T cells. In previous studies, the mechanism of Kyn-induced T cell suppression was poorly understood. Liu and colleagues reported that tumor repopulating cells could produce Kyn to mediate PD-1 upregulation in active T cells, resulting in immune suppression in the tumor microenvironment [42]. Consistently, our study provided evidence that Kyn derived from tumor cells mediated PD-1 expression in $CD8^+$ T cells in glioma, which further illustrated the underlying mechanism of Kyn-induced immune suppression. Much work has been done on IDO inhibitors for tumor elimination. Our work further suggested a mechanism where Kyn induced by TDO2 contributed to immunosuppression and cancer development. While immunotherapy targeting IDO was still not sufficient, it might be efficient for tumor inhibition.

It has been documented that AhR is an effective contributor to tumor progression, especially in breast cancer [43]. Nuclear translocation of AhR was capable of promoting p53-dependent transcription of the multidrug resistant gene MDR-1, resulting in drug resistance of tumor cells [44]. More importantly, the activated ligand AhR has been proposed to participate in the growth and metastasis of lung cancer cells, and inhibition of AhR contributes to significant anticancer effects in several tumor types [22, 26, 45]. We found that autocrine Kyn promoted the activation of AhR, which further facilitated the AKT/CREB pro-survival signaling pathway. To obtain evidence that the AhR/AKT pathway participated in glioma progression *in vivo*, the expression of AhR was examined in glioma tissues using TCGA databases and clinical samples from patients. As expected, a high correlation was observed between Kyn secretion and AhR expression in glioma tissues. And GO pathway enrichment suggested a role of AhR/AKT signaling pathway in glioma development. Our study further confirmed the role of AhR in tumor progression, in which AhR participated in tryptophan metabolism to promote glioma growth and invasion (**Figure 8**).

Conclusions

Taken together, our findings here suggested the correlation between tryptophan metabolism and glioma progression. Elevated Kyn levels induced by TDO2 promoted glioma cell proliferation and invasion through the AhR/AKT/

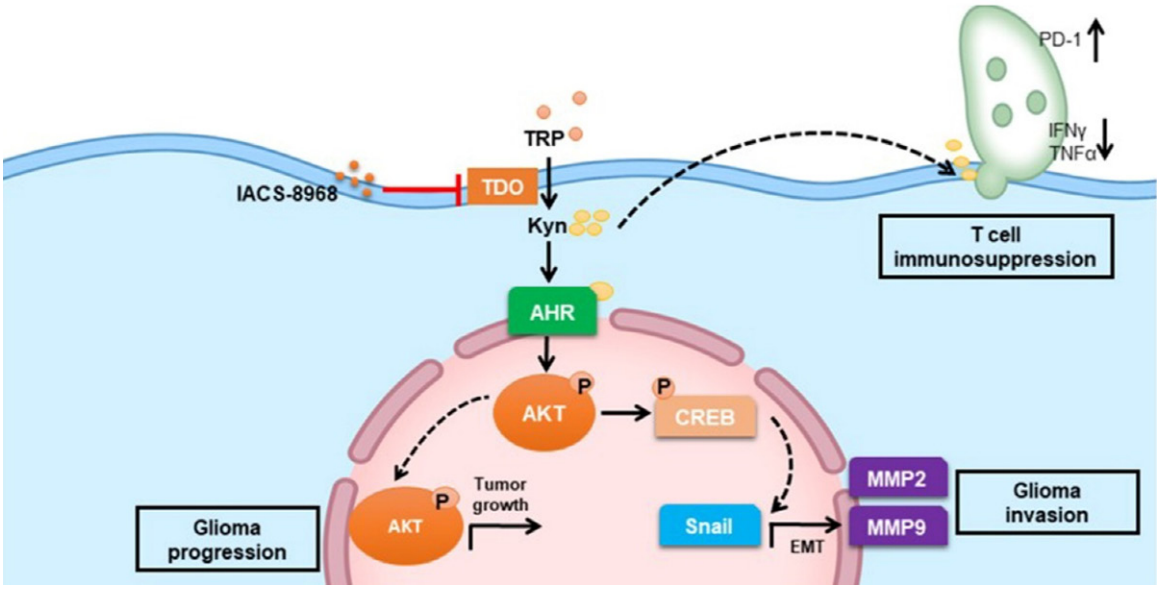

Figure 8. Proposed mechanism of TDO2 and tryptophan metabolites promote kynurenine/AhR signals to facilitate glioma progression and immunosuppression. tryptophan metabolite Kyn induced by TDO2 played a pivotal role in development of glioma via the AhR/AKT pro-survival signals and immunosuppressive effects, and provides novel strategy that the use of TDO2 inhibitor combing with chemotherapy might effectively synergize the elimination of glioma cells.

CREB signaling pathway, and repressed the anticancer responses of T cells. Targeting TDO2 efficiently suppressed cancer development and strengthened the cytotoxicity of chemotherapy for patient-derived glioma cells, which represents an innovative approach for glioma treatment.

Acknowledgements

Supported by National Natural Science Foundation of China (Grant No. 81802096), Foundation of Science and Technology Department of Sichuan province (Grant No. 2019YFS0398, 2019YFS0396), Luzhou Science and Technology Program (Grant No. 2020-JYJ-45).

Disclosure of conflict of interest

None.

Address correspondence to: Peizhi Zhou, Department of Neurosurgery, West China Hospital of Sichuan University, No. 37 Guoxue Alley, Chengdu 610041, Sichuan, China. Fax: +86-028-85422114; E-mail: peizhizhou@126.com

References

[1] Weller M, Wick W, Aldape K, Brada M, Berger M, Pfister SM, Nishikawa R, Rosenthal M, Wen PY, Stupp R and Reifenberger G. Glioma. Nat Rev Dis Primers 2015; 1: 15017.

[2] Lapointe S, Perry A and Butowski NA. Primary brain tumours in adults. Lancet 2018; 392: 432-446.

[3] Pace A, Dirven L, Koekkoek JAF, Golla H, Fleming J, Rudà R, Marosi C, Le Rhun E, Grant R, Oliver K, Oberg I, Bulbeck HJ, Rooney AG, Henriksson R, Pasman HRW, Oberndorfer S, Weller M and Taphoorn MJB; European Association of Neuro-Oncology palliative care task force. European Association for Neuro-Oncology (EANO) guidelines for palliative care in adults with glioma. Lancet Oncol 2017; 18: e330-e340.

[4] Bush NA, Chang SM and Berger MS. Current and future strategies for treatment of glioma. Neurosurg Rev 2017; 40: 1-14.

[5] Gusyatiner O and Hegi ME. Glioma epigenetics: from subclassification to novel treatment options. Semin Cancer Biol 2018; 51: 50-58.

[6] Omuro A and DeAngelis LM. Glioblastoma and other malignant gliomas: a clinical review. JAMA 2013; 310: 1842-1850.

[7] Woolf EC and Scheck AC. The ketogenic diet for the treatment of malignant glioma. J Lipid Res 2015; 56: 5-10.

[8] Zhou Y, Huang Y, Song X, Guo X, Pang J, Wang J, Zhang S and Wang C. Single-cell transcriptional profile of ACE2 in healthy and failing human hearts. Sci China Life Sci 2020; 64: 652-655.

[9] Peng Z, Liu C and Wu M. New insights into long noncoding RNAs and their roles in glioma. Mol Cancer 2018; 17: 61.
[10] Ruff M, Kizilbash S and Buckner J. Further understanding of glioma mechanisms of pathogenesis: implications for therapeutic development. Expert Rev Anticancer Ther 2020; 20: 355-363.
[11] Shi F, Zhou M, Shang L, Du Q, Li Y, Xie L, Liu X, Tang M, Luo X, Fan J, Zhou J, Gao Q, Qiu S, Wu W, Zhang X, Bode AM and Cao Y. EBV(LMP1)-induced metabolic reprogramming inhibits necroptosis through the hypermethylation of the RIP3 promoter. Theranostics 2019; 9: 2424-2438.
[12] Wettersten HI, Aboud OA, Lara PN Jr and Weiss RH. Metabolic reprogramming in clear cell renal cell carcinoma. Nat Rev Nephrol 2017; 13: 410-419.
[13] Biswas SK. Metabolic reprogramming of immune cells in cancer progression. Immunity 2015; 43: 435-449.
[14] Ryall JG, Cliff T, Dalton S and Sartorelli V. Metabolic reprogramming of stem cell epigenetics. Cell Stem Cell 2015; 17: 651-662.
[15] Pavlova NN and Thompson CB. The emerging hallmarks of cancer metabolism. Cell Metab 2016; 23: 27-47.
[16] Bose S, Allen AE and Locasale JW. The molecular link from diet to cancer cell metabolism. Mol Cell 2020; 78: 1034-1044.
[17] Vander Heiden MG and DeBerardinis RJ. Understanding the intersections between metabolism and cancer biology. Cell 2017; 168: 657-669.
[18] Opitz CA, Somarribas Patterson LF, Mohapatra SR, Dewi DL, Sadik A, Platten M and Trump S. The therapeutic potential of targeting tryptophan catabolism in cancer. Br J Cancer 2020; 122: 30-44.
[19] Platten M, Wick W and Van den Eynde BJ. Tryptophan catabolism in cancer: beyond IDO and tryptophan depletion. Cancer Res 2012; 72: 5435-5440.
[20] Yu CP, Song YL, Zhu ZM, Huang B, Xiao YQ and Luo DY. Targeting TDO in cancer immunotherapy. Med Oncol 2017; 34: 73.
[21] Sorgdrager FJH, Naudé PJW, Kema IP, Nollen EA and Deyn PP. Tryptophan metabolism in inflammaging: from biomarker to therapeutic target. Front Immunol 2019; 10: 2565.
[22] Cheong JE and Sun L. Targeting the IDO1/TDO2-KYN-AhR pathway for cancer immunotherapy - challenges and opportunities. Trends Pharmacol Sci 2018; 39: 307-325.
[23] Munn DH and Mellor AL. IDO in the tumor microenvironment: inflammation, counter-regulation, and tolerance. Trends Immunol 2016; 37: 193-207.
[24] Li F, Zhao Y, Wei L, Li S and Liu J. Tumor-infiltrating Treg, MDSC, and IDO expression associated with outcomes of neoadjuvant chemotherapy of breast cancer. Cancer Biol Ther 2018; 19: 695-705.
[25] Furue M, Hashimoto-Hachiya A and Tsuji G. Aryl Hydrocarbon receptor in atopic dermatitis and psoriasis. Int J Mol Sci 2019; 20: 5424.
[26] Murray IA, Patterson AD and Perdew GH. Aryl hydrocarbon receptor ligands in cancer: friend and foe. Nat Rev Cancer 2014; 14: 801-814.
[27] Shinde R and McGaha TL. The aryl hydrocarbon receptor: connecting immunity to the microenvironment. Trends Immunol 2018; 39: 1005-1020.
[28] Stockinger B, Di Meglio P, Gialitakis M and Duarte JH. The aryl hydrocarbon receptor: multitasking in the immune system. Annu Rev Immunol 2014; 32: 403-432.
[29] Gutiérrez-Vázquez C and Quintana FJ. Regulation of the immune response by the aryl hydrocarbon receptor. Immunity 2018; 48: 19-33.
[30] Swanson HI. DNA binding and protein interactions of the AHR/ARNT heterodimer that facilitate gene activation. Chem Biol Interact 2002; 141: 63-76.
[31] Guarnieri T. Aryl hydrocarbon receptor connects inflammation to breast cancer. Int J Mol Sci 2020; 21: 5264.
[32] Opitz CA, Litzenburger UM, Sahm F, Ott M, Tritschler I, Trump S, Schumacher T, Jestaedt L, Schrenk D, Weller M, Jugold M, Guillemin GJ, Miller CL, Lutz C, Radlwimmer B, Lehmann I, von Deimling A, Wick W and Platten M. An endogenous tumour-promoting ligand of the human aryl hydrocarbon receptor. Nature 2011; 478: 197-203.
[33] Bianchi-Smiraglia A, Bagati A, Fink EE, Affronti HC, Lipchick BC, Moparthy S, Long MD, Rosario SR, Lightman SM, Moparthy K, Wolff DW, Yun DH, Han Z, Polechetti A, Roll MV, Gitlin, II, Leonova KI, Rowsam AM, Kandel ES, Gudkov AV, Bergsagel PL, Lee KP, Smiraglia DJ and Nikiforov MA. Inhibition of the aryl hydrocarbon receptor/polyamine biosynthesis axis suppresses multiple myeloma. J Clin Invest 2018; 128: 4682-4696.
[34] Attafi IM, Bakheet SA and Korashy HM. The role of NF-κB and AhR transcription factors in lead-induced lung toxicity in human lung cancer A549 cells. Toxicol Mech Methods 2020; 30: 197-207.
[35] D'Amato NC, Rogers TJ, Gordon MA, Greene LI, Cochrane DR, Spoelstra NS, Nemkov TG, D'Alessandro A, Hansen KC and Richer JK. A TDO2-AhR signaling axis facilitates anoikis resistance and metastasis in triple-negative breast cancer. Cancer Res 2015; 75: 4651-4664.

[36] Dubrovska A, Hartung A, Bouchez LC, Walker JR, Reddy VA, Cho CY and Schultz PG. CXCR4 activation maintains a stem cell population in tamoxifen-resistant breast cancer cells through AhR signalling. Br J Cancer 2012; 107: 43-52.

[37] Kubli SP, Bassi C, Roux C, Wakeham A, Göbl C, Zhou W, Jafari SM, Snow B, Jones L, Palomero L, Thu KL, Cassetta L, Soong D, Berger T, Ramachandran P, Baniasadi SP, Duncan G, Lindzen M, Yarden Y, Herranz C, Lazaro C, Chu MF, Haight J, Tinto P, Silvester J, Cescon DW, Petit A, Pettersson S, Pollard JW, Mak TW, Pujana MA, Cappello P and Gorrini C. AhR controls redox homeostasis and shapes the tumor microenvironment in BRCA1-associated breast cancer. Proc Natl Acad Sci U S A 2019; 116: 3604-3613.

[38] Qiu Y, Qiu S, Deng L, Nie L, Gong L, Liao X, Zheng X, Jin K, Li J, Tu X, Liu L, Liu Z, Bao Y, Ai J, Lin T, Yang L and Wei Q. Biomaterial 3D collagen I gel culture model: a novel approach to investigate tumorigenesis and dormancy of bladder cancer cells induced by tumor microenvironment. Biomaterials 2020; 256: 120217.

[39] Quintana FJ. LeA(H)Rning self-control. Cell Res 2014; 24: 1155-1156.

[40] Merlo LMF, DuHadaway JB, Montgomery JD, Peng WD, Murray PJ, Prendergast GC, Caton AJ, Muller AJ and Mandik-Nayak L. Differential roles of IDO1 and IDO2 in T and B cell inflammatory immune responses. Front Immunol 2020; 11: 1861.

[41] Zhai L, Ladomersky E, Lenzen A, Nguyen B, Patel R, Lauing KL, Wu M and Wainwright DA. IDO1 in cancer: a gemini of immune checkpoints. Cell Mol Immunol 2018; 15: 447-457.

[42] Liu Y, Liang X, Dong W, Fang Y, Lv J, Zhang T, Fiskesund R, Xie J, Liu J, Yin X, Jin X, Chen D, Tang K, Ma J, Zhang H, Yu J, Yan J, Liang H, Mo S, Cheng F, Zhou Y, Zhang H, Wang J, Li J, Chen Y, Cui B, Hu ZW, Cao X, Xiao-Feng Qin F and Huang B. Tumor-repopulating cells induce PD-1 expression in CD8(+) T cells by transferring kynurenine and AhR activation. Cancer Cell 2018; 33: 480-494.

[43] Miret N, Zappia CD, Altamirano G, Pontillo C, Zárate L, Gómez A, Lasagna M, Cocca C, Kass L, Monczor F and Randi A. AhR ligands reactivate LINE-1 retrotransposon in triple-negative breast cancer cells MDA-MB-231 and non-tumorigenic mammary epithelial cells NMuMG. Biochem Pharmacol 2020; 175: 113904.

[44] To KK, Yu L, Liu S, Fu J and Cho CH. Constitutive AhR activation leads to concomitant ABCG2-mediated multidrug resistance in cisplatin-resistant esophageal carcinoma cells. Mol Carcinog 2012; 51: 449-464.

[45] Trikha P and Lee DA. The role of AhR in transcriptional regulation of immune cell development and function. Biochim Biophys Acta Rev Cancer 2020; 1873: 188335.

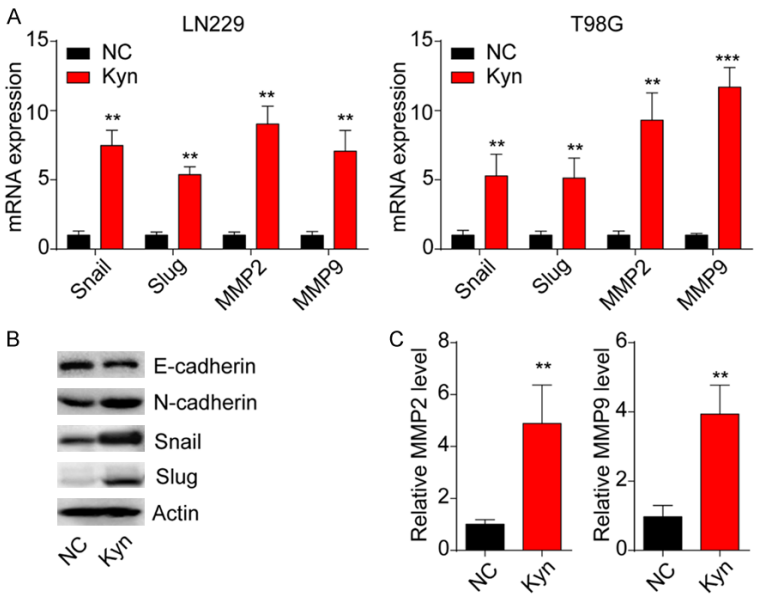

Figure S1. A. Relative expression of Snail, Slug, MMP2 and MMP9 at mRNA level in LN229/T98G cells treated with NC or Kyn (100 μM). B. Western blotting of E-cadherin, N-cadherin, Snail and Slug in tumor tissues isolated from LN229-bearing mice treated with NC or Kyn (2 μg). Tumor tissues were collected in 3 days after Kyn treatment. C. Realative MMP2 and MMP9 in tumor tissues isolated from LN229-bearing mice treated with NC or Kyn (2 μg). Tumor tissues were collected in 3 days after Kyn treatment. NC, normal saline, **P<0.01, ***P<0.001.